

An Image-based Multiproxy Palpation Algorithm for Patient-Specific VR-Simulation

Dirk FORTMEIER^{a,b,1}, Andre MASTMEYER^a and Heinz HANDELS^a

^a*Institute of Medical Informatics, University of Lübeck, Lübeck, Germany*

^b*Graduate School for Computing in Medicine and Life Sciences, University of Lübeck*

Abstract. Palpation is the first step for many medical interventions. To provide an immersive virtual training and planning environment, the palpation step has to be successfully modeled and simulated. Here, we present a multiproxy approach that calculates friction and surface resistance forces for multiple contact points on finger tips or virtual tools like ultrasound probes and displays the resulting force and torque on a 6DOF haptic device. No manual or time intensive segmentation of patient image data is needed to create a simulation based on CT data and thus our approach is usable for patient-specific simulation of palpation.

Keywords. haptic simulation, palpation, ultrasound haptics

Introduction

Before performing a needle insertion, a palpation of the anatomical site is done in the first place. For example, in preparation of the Seldinger technique, first the femoral artery has to be found in which a needle shall be inserted. Palpation simulation for that aim was presented recently by [1] and [2]. Other needle insertion interventions that require palpation are lumbar puncture, where the iliac crest and spinal processes have to be palpated before a needle is inserted into the spinal canal, or percutaneous transhepatic cholangiodrainage (PTCD), where the intercostal spaces have to be found before puncturing the liver and bile ducts. The simulation framework of our current project focuses on the PTCD.

Most haptic simulations of palpation need surface representation of the virtual patients, which require preprocessing steps such as segmentation of the patient's volumetric image data. Furthermore, soft-tissue deformation algorithms as FEM additionally require a suitable tetrahedra representation of the patient. Another approach is presented by [3]. There, organs are represented by mathematical functions, which are used to render haptic force output.

Ideally, a simulation that could be used for preoperative training and planning should work without an intermediate step of surface and tissue reconstruction that needs manual interaction. So our aim is to directly work on patient image data obtained by computed

¹Corresponding Author: Dirk Fortmeier, Institute of Medical Informatics, Ratzeburger Allee 160, 23538 Lübeck, Germany; E-mail: fortmeier@imi.uni-luebeck.de

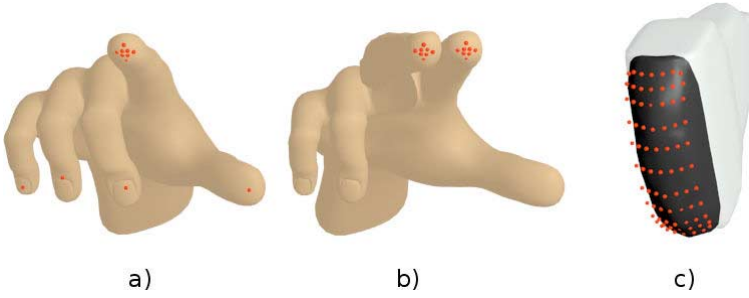


Figure 1. Placement of contact points on different tools: (a) Hand with one palpating finger, (b) hand with two palpating fingers, (c) ultrasound probe.

tomography (CT) and use it for visual and haptic rendering. Haptic interaction with volumetric data in general has previously been done by [4] and Euclidean distance maps for haptic navigation have been used by [5]. In this paper, we extend our previous work on palpation simulation [6] and contribute an easy to implement and fast to compute multiproxy approach for (1) surface resistance forces, (2) surface friction forces, (3) force feedback of internal structures such as bone and (4) torque forces. For the computation of skin surface forces and force feedback of bony structures, we rely on Euclidean distance maps. These distance maps are obtained from skin and bone masks created by simple region growing and thresholding.

The proxies used are connected to contact points distributed on the tip of the virtual fingers or on the surface of virtual tools and the sum of forces and torques is displayed to the user via a 6DOF haptic device. Among others, the algorithm can be used for the computation of forces for a single finger, two combined fingers or tools such as ultrasound probes (Fig. 1).

The paper is organized as follows: First, we explain how the surface resistance force for each contact point is calculated and how the force of internal structures is simulated. Afterwards, we present our method to create friction and dragging forces. We present different set-ups of the positioning of the contact points and discuss parameters for simulation of palpation with a finger and ultrasound probe. In the end, we analyze and present the behavior of our haptic algorithm in our simulation framework.

Methods and Materials

Our approach is based on a patient’s volumetric computed tomography data. First, we perform thresholding and simple region growing operations to segment the patient’s body and bony structures. From this, we compute two Euclidean distance maps \mathbf{D}_{surf} and \mathbf{D}_{bone} which resemble the distance of the elements of the maps to the patient’s skin surface and bone surface respectively; by convention, negative values in the maps indicate that the according voxel is outside the structure, positive values indicate the inside.

In the following, we will describe how force and torque are calculated for a single contact point (Fig. 2): The position of a contact point \mathbf{x} in each time step is determined by its position in its reference frame and the position and orientation of the haptic device. For this position, a surface resistance force \mathbf{f}_{surf} is computed dependent on the distance

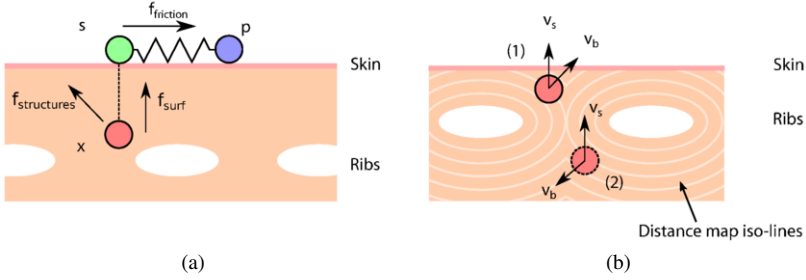


Figure 2. Computation of the force feedback for a single contact point. (a) Calculation of the force acting on a contact node is split into three parts: Skin resistance force f_{surf} , force caused by internal bone structures $f_{structures}$ and skin friction force $f_{friction}$. (b) The direction of the bone force has to be chosen carefully: At (1), the gradient of the bone distance map points towards the patient’s skin. After passing the intercostal spaces at (2), the gradient points in the opposite direction. Using only the direction the gradient thus would cause a “pop-thru” effect.

of \mathbf{x} towards the skin and the negative gradient of the surface distance image \mathbf{v}_s , which points towards the skins surface:

$$\mathbf{v}_s = -\frac{\nabla \mathbf{D}_{surf}(\mathbf{x})}{\|\nabla \mathbf{D}_{surf}(\mathbf{x})\|} \quad (1)$$

$$\mathbf{f}_{surf} = f_{surf}(\mathbf{D}_{skin}(\mathbf{x})) \cdot \mathbf{v}_s \quad (2)$$

We base the function $f_{surf}(x)$, which relates surface indentation to the resistance force, on the data presented in [1] for femoral artery palpation. A curve fitting with a cubic function gave:

$$f_{surf}(x) = (1.78 \cdot 10^{-2}x^3 + 3.82 \cdot 10^{-3}x^2 + 2.28 \cdot 10^{-4}x) \cdot u(x) \quad (3)$$

with $u(x)$ denoting the Heaviside function. This force is similar to a penalty force based collision handling scheme and thus is theoretically prone to “pop-thru” effects [7]. In reality, we found this not to be a problem because of the size of the palpated object (the whole patient body) and the high resistance force after a small amount of indentation ($>20\text{N}$ after 40mm indentation) and the availability of a high force haptic device.

The force for the internal structures (bone) is calculated by first calculating a direction of the force based on the negative gradient of the bone surface distance map $\mathbf{v}_b = -\frac{\nabla \mathbf{D}_{bone}(\mathbf{x})}{\|\nabla \mathbf{D}_{bone}(\mathbf{x})\|}$. In case the inner product of \mathbf{v}_s and \mathbf{v}_b is negative, it is very likely that the position \mathbf{x} is past the intercostal spaces (see Fig. 2b) and thus the bone force would “pop-thru”. This is prevented by the choice of the direction \mathbf{d}_{bone} of the force in a way that it never points away from the skin:

$$\mathbf{d}_{bone} = \begin{cases} \mathbf{v}_b & \text{if } \mathbf{v}_b \mathbf{v}_s > 0 \\ \mathbf{v}_b - 4 \cdot \mathbf{v}_s (\mathbf{v}_b \mathbf{v}_s) & \text{otherwise} \end{cases} \quad (4)$$

Using a heuristic bone force $f_{bone}(x) = 20 \cdot \left(\frac{x}{5}\right)^{-3} u(x)$, the force is computed by

$$\mathbf{f}_{structures} = f_{bone}(-\mathbf{D}_{bone}(\mathbf{x})) \frac{\mathbf{d}_{bone}}{\|\mathbf{d}_{bone}\|} \quad (5)$$

In contrast to the previous forces, lateral dragging and friction forces rely on a proxy-based scheme [7]. A surface position $\mathbf{s} = \mathbf{x} - \mathbf{D}_{\text{surf}}(\mathbf{x})\mathbf{v}_s$ on the virtual skin is calculated by using the surface distance map. This surface position is then connected to a virtual proxy position \mathbf{p} (see Fig. 2a), which is updated in each successive time step t by the friction law of [8]:

$$\mathbf{p}_t = \begin{cases} \mathbf{s}_t - \frac{\mathbf{d}}{\|\mathbf{d}\|} z_{\text{max}} & \text{if } \alpha(\|\mathbf{d}\|) \|\mathbf{d}\| > 1 \\ \mathbf{p}_{t-1} + |\mathbf{s}_t - \mathbf{s}_{t-1}| \alpha(\|\mathbf{d}\|)(\mathbf{d}) & \text{otherwise} \end{cases} \quad (6)$$

with $\mathbf{d} = \mathbf{s}_t - \mathbf{p}_{t-1}$.

We use the proposed version of $\alpha(z) = \frac{1}{z_{\text{max}}} \frac{z^8}{z_{\text{stick}}^8 + z^8}$ of [8] but modify the values of z_{max} and z_{stick} depending on the surface resistance force acting on the contact point:

$$\mathbf{f}_n = (\mathbf{f}_{\text{surf}} + \mathbf{f}_{\text{structures}}) \quad (7)$$

$$z_{\text{max}} = \begin{cases} c \mathbf{f}_n \cdot \mathbf{v}_s + 1 & \text{if } \mathbf{f}_n \cdot \mathbf{v}_s < 0 \\ 1 & \text{otherwise} \end{cases} \quad (8)$$

$$z_{\text{stick}} = z_{\text{max}} - 1 \quad (9)$$

To compute the actual force $\mathbf{f} = \mathbf{f}_{\text{surf}} + \mathbf{f}_{\text{friction}} + \mathbf{f}_{\text{structures}}$ acting on the contact point, Hooke's law is used to calculate the force $\mathbf{f}_{\text{friction}} = k(\mathbf{p} - \mathbf{s})$ of a virtual spring that connects the surface point and the proxy.

Torque is simply computed by the lever arm defined by the position of the contact point and the haptic device position:

$$\boldsymbol{\tau} = (\mathbf{x} - \mathbf{x}_{\text{device}}) \times \mathbf{f} \quad (10)$$

The final force and torque rendered to the user is the average of forces and torques of all n contact points that are considered to be on the patient's skins surface:

$$\mathbf{f}_{\text{device}} = \frac{1}{n} \sum_{i=0}^n \mathbf{f}_i \quad (11)$$

$$\boldsymbol{\tau}_{\text{device}} = \frac{1}{n} \sum_{i=0}^n \boldsymbol{\tau}_i \quad (12)$$

Visual rendering of the patient's volume data is done by a custom volume renderer written in Nvidia CUDA that supports a basic spherical shadow to improve spatial interaction for the user. Visual deformations of the skin invoked by the palpating fingertip are computed with the ChainMail algorithm [9] and methods of [10]. A displacement vector on the contact point of the fingertip on the patient's skin is needed, which we compute from the mean of the n points \mathbf{x}_i in contact with the skin and the mean of the corresponding proxies \mathbf{p}_i :

$$\mathbf{u} = \frac{1}{n} \sum_{i=0}^n \mathbf{p}_i - \mathbf{x}_i \quad (13)$$

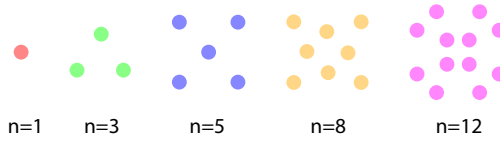


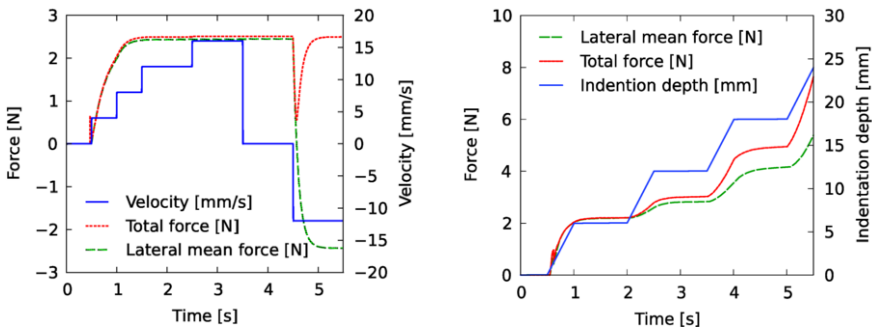
Figure 3. Spatial arrangement of different contact point set-ups on the fingertip.

Note that this could be used in a finite element or mass-spring approach as well by applying the fixed offset $-\mathbf{u}$ to a node of a mesh closest to the mean of the proxy points or by creating a force field from the displacements defined by each contact point and its corresponding proxy.

In our PTCF simulator, two interactions with the patient’s skin are included: Palpation with the finger to find the intercostal spaces and positioning and alignment of an ultrasound probe to guide a needle into the bile duct. Using an array placement of nodes as shown in Fig. 1 gives suitable skin resistance and internal structure force feedback for different tools. Nevertheless, friction forces are much different for interaction of fingertip and skin compared to the frictional interaction of an ultrasound probe and skin. In general, for ultrasound-probing a lubricant is applied to increase the area of contact but more importantly it reduces friction, which leads to the need for different parameters for the friction model. Setting $c = 2.0$ and $k = 0.4$ gave plausible results for palpation with the fingertip. For ultrasound probing, we consider values of $c = 0.4$ and $k = 0.3$ to be a reasonable choice. The large difference in two values for c reflects that with an ultrasound probe, nearly no tissue dragging occurs compared to a fingertip.

Results

To show the general properties of our algorithm, a cubic phantom was palpated by using a predefined haptic device trajectory as in [11]. Instead of using an actual haptic device, the virtual device tip is moved on a predefined path to obtain deterministic and reproducible results. Two scenarios are considered: First, a path with fixed lateral motion on



(a) Behavior of the algorithm when palpating with changing velocity and fixed tissue indentation. (b) Behavior of the algorithm when palpating with changing tissue indentation and fixed velocity.

Figure 4. Mean lateral friction force and total forces for a lateral palpating movement of the haptic device. Data has been obtained on a virtual cubic phantom and by using a predefined path of the haptic device tip.

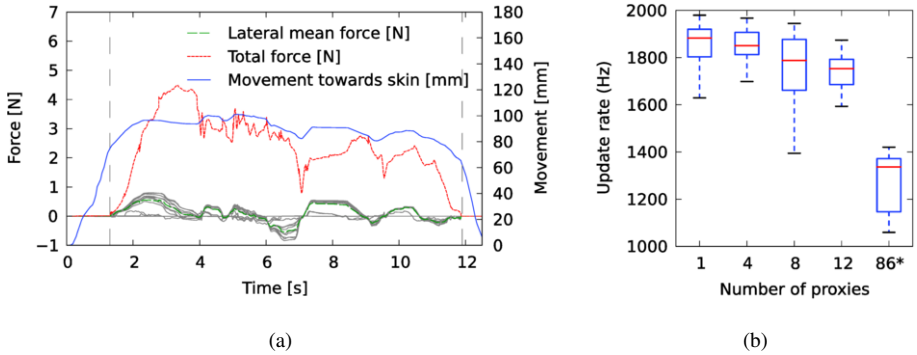


Figure 5. Data obtained in a simulation with real patient data. (a) Blue curve (continuous): movement of the fingertip in direction of indentation while palpating. Green curve (dashed): resulting mean lateral friction force displayed with the 6DOF haptic device. Forces of individual contact points are displayed by the gray curves. At the peak at $t = 2.5s$, the user’s fingertip was near a rib, whereas the peaks at $t = \{5, 8, 10\}s$, the tip has been between the intercostal spaces. Dashed lines indicate beginning and end of palpation. (b) Different update rates of the algorithm based on the number of proxies with mean, quartiles and 1.5 IQR. (*) indicates that the ultrasound proxy set-up (Fig. 1c) was used.

the phantom’s surface and increasing indentation depth was used. The second scenario uses a fixed indentation and changes the velocity while moving on the surface. Contact points have been placed according to Fig. 3 for different numbers of contact points. The results can be seen in Fig. 4; lateral friction forces clearly scale with the indentation depth of the palpating finger and on stationary movement. No creep of contact surfaces occurs, which would happen if only viscous damping would be used for friction simulation. Since no local tissue deformation affects the contact points, forces have been the same for all contact points and thus the total forces do not vary for different numbers of contact points. This confirms another desirable property of our algorithm: friction forces are independent on the number of contact points and the size of the area in contact.

Finally, Fig. 5a shows a plot of forces obtained in the simulator with real patient data and Fig. 5b shows reasonable update rates (between 1-2kHz) of the algorithm for different numbers of proxies obtained during $n = 5$ palpations. The screenshot of the running simulator (Fig. 6) shows the finger before and while palpating and deforming the tissue. Deformations caused by indentation of the palpating finger can be seen clearly but deformations caused by friction or “tissue dragging” are harder to identify. This is caused by the homogeneous rendering of the skin surface through volume rendering.

Using our algorithm for the computation of forces for ultrasound probing was successful and enables the user to align the virtual probe with the intercostal spaces.

Conclusions

We presented a multiproxy palpation algorithm that can be used to palpate virtual patients based on CT volume data without time-consuming segmentation or mesh preprocessing. The algorithm can be used to palpate with a virtual hand or ultrasound probe.

In the future, we would like to include forces acting on the proxies dependent on the deformations of tissue. To make other internal structures different from bone palpable,

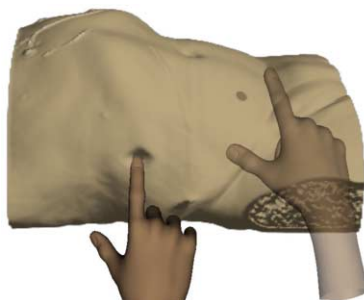


Figure 6. Screenshot of the simulation with real patient data. The left hand palpates the intercostal spaces. Deformations on the skin and inside the patient are computed by the ChainMail algorithm. The semitransparent hand on the right demonstrates the spherical shadow of the finger tip, which helps to visualize and indicate the spatial position of the haptic device.

we want to extend our method to distance maps created from rough (semi-)automatic segmentations.

Acknowledgment

This work is supported by the German Research Foundation (DFG, HA 2355/10-1) and the Graduate School for Computing in Medicine and Life Sciences.

References

- [1] T. Coles, N. John, D. Gould, and D. Caldwell, "Integrating Haptics with Augmented Reality in a Femoral Palpation and Needle Insertion Training Simulation," *IEEE Transactions on Haptics*, vol. 4, no. 3, pp. 199–209, 2011.
- [2] S. Ullrich and T. Kuhlen, "Haptic Palpation for Medical Simulation in Virtual Environments," *IEEE Transactions on Visualization and Computer Graphics*, vol. 18, no. 4, pp. 617–25, 2012.
- [3] S. Yasmin and A. Sourin, "Image-Based Virtual Palpation," *Transactions on Computational Science XVIII*, pp. 61–80, 2013.
- [4] K. Lundin, B. Gudmundsson, and A. Ynnerman, "General Proxy-based Haptics for Volume Visualization," in *World Haptics Conference*, pp. 557–560, 2005.
- [5] D. Bartz and Ö. Gürvit, "Haptic Navigation in Volumetric Datasets," in *Proceedings of PHANTOM User Research Symposium*, pp. 43–47, 2000.
- [6] D. Fortmeier, A. Mastmeyer, and H. Handels, *Image-based Palpation Simulation with Soft Tissue Deformations using ChainMail on the GPU*. BVM 2013 (German Conference on Medical Image Processing), Heidelberg: Springer Verlag, Berlin, 2013.
- [7] D. C. Ruspini, K. Kolarov, and O. Khatib, "The Haptic Display of Complex Graphical Environments," in *Proceedings of the 24th Annual Conference on Computer Graphics and Interactive Techniques*, pp. 345–352, ACM Press/Addison-Wesley Publishing Co., 1997.
- [8] V. Hayward and B. Armstrong, "A New Computational Model of Friction Applied to Haptic Rendering," in *Experimental Robotics VI*, pp. 404–412, Springer London, 2000.
- [9] S. Gibson, "3D Chainmail: A Fast Algorithm for Deforming Volumetric Objects," in *Proc Interactive 3D Graphics*, (New York), pp. 149–ff, ACM, 1997.
- [10] D. Fortmeier, A. Mastmeyer, and H. Handels, "Image-based Soft Tissue Deformation Algorithms for Real-time Simulation of Liver Puncture," *Current Medical Imaging Reviews*, vol. 9, pp. 154–165, 2013.
- [11] A. Mastmeyer, D. Fortmeier, and H. Handels, *Direct Haptic Volume Rendering in Lumbar Puncture Simulation*. Stud Health Technol Inform, 173, IOS Press, 2012.